Fiber-optic Fabry−Pérot strain sensor based on graded-index multimode fiber

Tian Zhao (赵 天), Yuan Gong (龚 元), Yunjiang Rao (饶云江)*, Yu Wu (吴 宇), Zengling Ran (冉曾令), and Huijuan Wu (吴慧娟)

Key Laboratory of Optical Fiber Sensing and Communications (Education Ministry of China), University of Electronic Science and Technology of China, Chengdu 611731, China

**Corresponding author: yjrao@uestc.edu.cn*

Received October 13, 2010; accepted January 14, 2011; posted online April 18, 2011

By using a graded-index multimode fiber (GI-MMF) with a relatively flat index profile and high refractive index of the fiber core, a microextrinsic fiber-optic Fabry−Pérot interferometric (MEFPI) strain sensor is fabricated through chemical etching and fusion splicing. Higher reflectance of the microcavity is obtained due to the less-curved inner wall in the center of the fiber core after etching and higher index contrast between the GI-MMF core and air. The maximum reflection of the sensor is enhanced 12 dB than that obtained by etching of the Er- or B-doped fibers. High fringe contrast of 22 dB is obtained. The strain and temperature responses of the MEFPI sensors are investigated in this experiment. Good linearity and high sensitivity are achieved, with wavelength-strain and wavelength-temperature sensitivities of 7.82 pm/$\mu\varepsilon$ and 5.01 pm/°C, respectively.

OCIS codes: 060.2370, 120.2230.

doi: 10.3788/COL201109.050602.

Fiber-optic sensors are being widely used nowadays due to their advantages over traditional sensors. Specifically, fiber-optic Fabry−Pérot interferometric (FPI) sensor[1−7] has been extensively investigated. In the past decade, the laser micromachining[8,9] and chemical etching techniques[10−15] were used to fabricate microextrinsic fiber-optic FPI (MEFPI) sensors. The laser micromachining technique is well controlled and can fabricate MEFPIs with high reproducibility. However, the technique is expensive and the relative position between the mask and the fiber to be processed needs to be adjusted precisely. The chemical etching method is cost-effective and has great potential for mass production. Cibula *et al.* fabricated their sensors in four steps: fusion splicing the graded-index multimode fiber (GI-MMF) to a single-mode fiber (SMF), cleaving the GI-MMF to the desired length, chemically etching the GI-MMF, and fusion splicing the etched fiber end to another SMF[15]. The cavity length of the sensor was determined by the GI-MMF length, which was controlled by a cleaver with a high-resolution microstage and an optical microscope. In our experiment, the fabrication procedure was greatly simplified, and the cavity length was controlled by the etching rate and time, which could be easily controlled with high precision.

In our previous work, we developed the MEFPI strain sensors by chemically etching the Er- and B-doped fibers[10]. The fringe contrast of the MEFPI sensors based on the Er-doped fibers was improved by a mixed etching solution and a relatively large discharge current. However, the maximum intensity of the reflective spectrum was small as the reflectances of both surfaces were very low. Recently, we fabricated hybrid FPI sensors by using the periodic effect of the GI-MMF, and FPI sensors of this kind were promising candidates for sensing refractive index accurately[11]. In this experiment, MEFPI sensors were fabricated by chemically etching a GI-MMF with a relatively flat index profile and high refractive index of the fiber core. Due to the large core diameter and high refractive index of the fiber core, both the maximum reflection of the sensor and the fringe contrast were enhanced, which was important for improving the performance of sensors. Both the strain and temperature characteristics of the MEFPI sensors were investigated and high sensitivity to strain was verified.

The GI-MMF used in our experiment was Model GI 105/125-30/250 from YOFC Ltd., China. The diameter of the fiber core was 105 μm. The numerical aperture (NA) was about 0.30, measured by the manufacturer. The nominal delta was calculated to be approximately 2.1% by using the equation $\Delta = (n_1 - n_2)/n_1$, where n_2, the refractive index of the fiber cladding (pure silica), was calculated to be 1.444 at 1.55 μm by the Sellmeier equation, and n_1, the maximum refractive index of the fiber core, was determined to be 1.475 by the NA and n_2. The index profile of the GI-MMF was quasi-quadratic and noted as GI-MMF-1; thus, the light propagated periodically along the fiber axis and the light trace was approximately sinusoidal function (Fig. 1). The index profile of another GI-MMF (Model GI 62.5/125-27/250, YOFC Ltd., China), which was used in our previous work[11], noted as GI-MMF-2 for comparison. The NA was about 0.275, measured by the manufacturer. Unlike our previous work, the periodic focusing effect along the GI-MMF was not used. The high refractive index of the fiber core was used to increase the reflectance of the second surface of the fiber-optic Fabry–Pérot cavity. As the second surface was curved, there was indeed a focusing effect similar to that of a concave reflective mirror.

The fabrication process of the MEFPI sensor presented is simple and cost-effective. Firstly, the cleaved GI-MMF was dipped into 40% HF acid and chemically etched for 1.5 min. A microcavity was formed on the GI-MMF end due to the etching rate of the fiber core ($V_{\rm core}$) that was higher than that of the cladding ($V_{\rm clad}$). The fiber cladding was generally made of pure SiO_2, and the

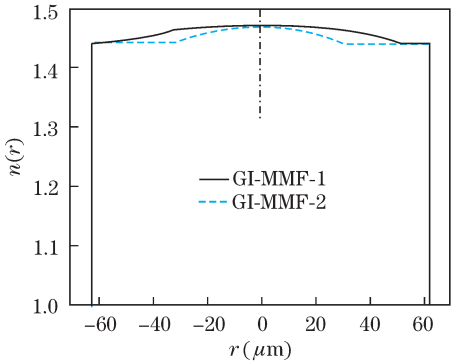

Fig. 1. Refractive index profile of two kinds of GI-MMF.

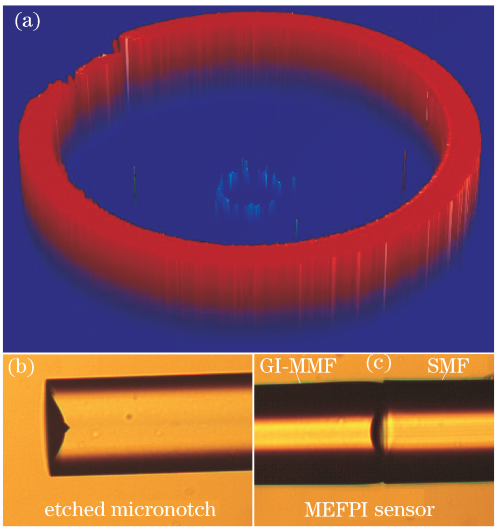

Fig. 2. (a) 3D profiles, (b) microscopic image of etched GI-MMF fiber end, and (c) microscopic image of MEFPI sensor.

fiber core of the GI-MMF we used was highly doped with GeO_2. The chemical equations of etching SiO_2 and GeO_2 are[16,17]

$$SiO_2 + 6HF = 2H_3O^+ + SiF_6^{2-}, \quad (1)$$

$$GeO_2 + 6HF = 2H_3O^+ + GeF_6^{2-}. \quad (2)$$

The dissociation energy of the Si-O bond, 799.6 kJ/mol, is larger than that of the Ge-O bond, 660.3 kJ/mol[10]. Thus, HF acid is more likely to chemically react with the fiber core. The three-dimensional (3D) surface profiles and the microscopic image of the etched GI-MMF are shown in Figs. 2(a) and (b), respectively. Secondly, the etched fiber was immersed into the deionized water for 15 min to wash away the residual etchant and then dried. Thirdly, the etched GI-MMF cavity with a depth of 25 μm was fusion spliced to a common SMF to form a MEFPI sensor (Fig. 2(c)). After fusion splicing, the cavity length, i.e., the spacing between the SMF end and the bottom of the etched microcavity, was measured to be 17.5 μm by an optical microscope. The cavity length was smaller than the depth of the etched cavity after etching, 25 μm, which was probably induced by the compression of the cavity during splicing due to the overlap of fibers.

A typical reflective spectrum of the MEFPI sensor is shown in Fig. 3. The free spectral range (FSR) was measured to be about 80 nm. The effective cavity length of the air gap was calculated to be approximately 15 μm by using the equation $L_0 = \lambda_1\lambda_2/4(\lambda_1 - \lambda_2)$, where λ_1 and λ_2 were the resonant wavelengths of the minimum and maximum intensities of the reflective spectrum (red online), respectively. The effective cavity length of the air gap was smaller than the cavity length measured by the optical microscope, 17.5 μm, due to the curved surface of the microcavity and the measurement errors of the FSR of the reflective spectrum. A maximum visibility of 22 dB was obtained, which was better than that of MEFPIs fabricated by a femtosecond laser, for example, 14 dB in Ref. [9], and comparable to that of MEFPIs fabricated by chemically etching Er-doped fibers, for example, 24 dB in Ref. [10] and 19 dB in Ref. [18].

MEFPI sensors fabricated by this method have several advantages over the sensors fabricated by the chemical etching method. One of the most obvious advantages is that the maximum reflection of the sensor, −15 dB, is much larger than that of the MEFPI sensors fabricated by chemically etching Er- or B-doped fibers, −28 dB, while the fringe contrast of the reflective spectrum is still high, 22 dB. As the doped region of the GI-MMF, i.e., the fiber core with a diameter of 105 μm, is much larger than that of the Er- or B-doped SMFs, <10 μm, the diameter of the etched cavity at the GI-MMF end is larger than that etched at the end of Er- or B-doped SMFs. When fusion splicing the etched fiber to a SMF, the collapse of the etched Er- or B-doped SMFs might lead to the decrement of the reflectance of the SMF end. However, this effect can be reduced by using the GI-MMF as the etched cavity is much larger than the diameter of the SMF and filled with air. Furthermore, the roughness of the etched cavity was reduced during the electric discharge and led to lower scattering losses. On the other hand, by using the GI-MMF with a high NA, the maximum refractive index of the fiber core was $n_1 = 1.475$ and the reflectance of the etched cavity was calculated to be 3.70% by the Fresnel equation $R = [(n_1-1)/(n_1+1)]^2$. This increment in the reflectance could cause an enhancement in the fringe contrast of the reflective spectrum since the reflectance of the two surfaces gets closer.

The characteristics of the reflective spectrum of the MEFPI sensor were greatly influenced by the optical path length (OPL). The longer cavity decreased recoupling efficiency of light that passed through the cavity due

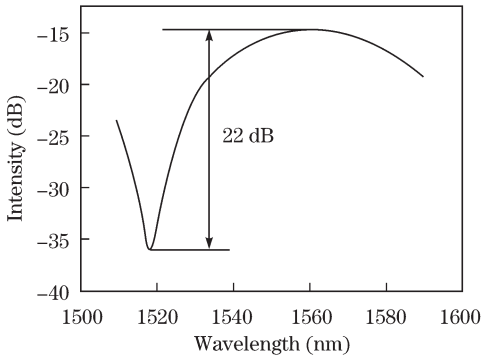

Fig. 3. Typical reflective spectrum of MEFPI sensor.

to the beam divergence. Different depths of cavity after etching resulted in different shapes of the inner cavity wall, which could affect the reflectance of that surface. The changes in strain or temperature led to changes in the cavity length of the sensor, thus inducing changes in the OPL. Therefore, the strain and temperature could be determined by measuring the wavelength shift of the reflective spectra.

The experimental setup used for testing the strain responses of the MEFPI sensor is shown in Fig. 4. The reflection of the MEFPI sensor was monitored by using a high-accuracy optical spectrum analyzer (Model Si720, Micron Optics, USA) with a wavelength scanning range of 1510−1590 nm and a wavelength resolution of 2.5 pm. The strain responses of the GI-MMF-based MEFPI sensors were investigated at room temperature (25 °C). Typical reflective spectra of the MEFPI sensor under strains of 0, 422, and 845 $\mu\varepsilon$ are shown in Fig. 5.

The experimental setup used for testing the temperature responses of the MEFPI sensor was similar to that given in Fig. 4, except that the MEFPI sensor was put into an experimental furnace (Model WD7005, Chongqing Action Experimental Equipment Co., China), which controlled the temperature in the range of −70 °C−130 °C, with a resolution of 0.1 °C. The test was measured from 90 °C to 10 °C, with a temperature interval of 10 °C.

The wavelength shift of the reflective spectrum is shown as a function of the applied strain and temperature in Fig. 6. The wavelength-strain sensitivity is 7.82 pm/$\mu\varepsilon$ and the linearity is 0.99982. The performance of the MEFPI sensor presented might be further improved by optimizing the etching time and the fusion parameters. The mechanical strength of the MEFPI sensor is good and can stand a maximum strain of 3760 $\mu\varepsilon$, more than twice

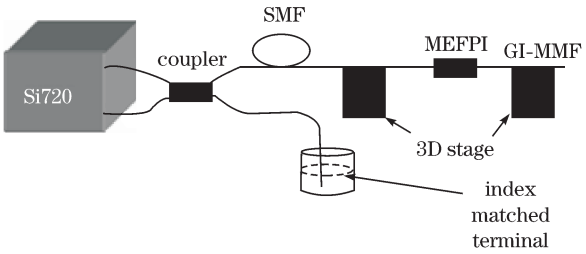

Fig. 4. Schematic diagram of the experimental setup for measuring strain response of MEFPI sensor.

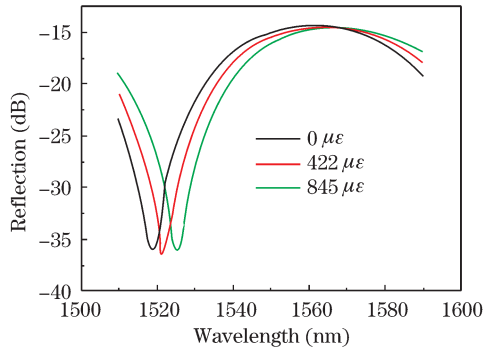

Fig. 5. Reflective spectra of MEFPI sensor with strain of 0, 422, and 845 $\mu\varepsilon$.

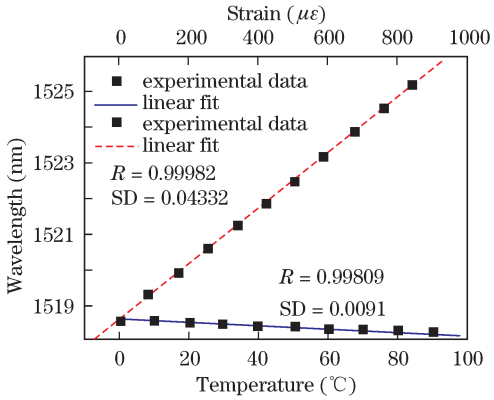

Fig. 6. Wavelength shift of reflective spectra of MEFPI sensor as function of strain and temperature.

that of the SMF-based MEFPI, 1400 $\mu\varepsilon$[17], and comparable to that of MEFPIs fabricated by chemically etching Er-doped fibers, about 3000 $\mu\varepsilon$[10]. The wavelength-temperature sensitivity is 5.01 pm/°C and the linearity is 0.99809. The temperature sensitivity of the sensor can be reduced by using the air gap cavity. As the temperature increases, the material expansion of the fiber cladding tends to extend the cavity length, while the material expansion of the fiber core tends to reduce the cavity, i.e., the two factors compensate each other and the temperature sensitivity can be reduced. This effect has been widely used to produce temperature-insensitive FPI sensors that can be used to measure the pressure or strain without temperature compensation[10,19,20].

Experimental results indicate that this sensor can measure either strain or temperature. The temperature-induced strain error is 0.64 $\mu\varepsilon$/°C. That is, a temperature fluctuation of 30 °C in the field environment introduces a strain error of only 19 $\mu\varepsilon$. Therefore, the temperature compensation would not be necessary if a relatively large strain is to be measured. In order to completely eliminate the influence of temperature variation on the strain measurement when such a sensor is used as a strain sensor, another temperature sensor should be used to compensate the thermal effect.

In conclusion, MEFPI sensors have been fabricated by chemically etching the GI-MMF with a relatively flat index profile and high refractive index of the fiber core and then fusion splicing the etched fiber to a SMF. The fabrication process is simple, cost-effective, and promising for mass production. The strain and temperature responses of the MEFPI sensors have been investigated in this experiment. The performance of the sensor, mainly in its maximum reflection, strain and temperature sensitivity, has been improved.

This work was supported by the State Key Laboratory of Advanced Optical Communication Systems and Networks, China.

References

1. X. Wan and H. F. Taylor, Opt. Lett. **27,** 1388 (2002).
2. J. Zhang, G. D. Peng, L. Yuan, and W. Sun, Opt. Lett. **32,** 1833 (2007).
3. Q. Wang and Q. Yu, Chin. Opt. Lett. **8,** 266 (2010).

4. M. Yang, Y. Sun, X. Li, and D. Jiang, Chin. Opt. Lett. **8(S),** 189 (2010).
5. T. Hu, Y. Zhao, X. Li, J. Chen, and Z. Lü, Chin. Opt. Lett. **8,** 392 (2010).
6. Y. Jiang and W. Ding, Photon. Sensor. **1,** 62 (2011).
7. Q. Yu and X. Zhou, Photon. Sensor. **1,** 72 (2011).
8. Z. L. Ran, Y. J. Rao, H. Y. Deng, and X. Liao, Opt. Lett. **32,** 3071 (2007).
9. T. Wei, Y. Han, H. Tsai, and H. Xiao, Opt. Lett. **33,** 536 (2008).
10. Y. Gong, Y. Rao, Y. Guo, Z. Ran, and Y. Wu, IEEE Photon. Technol. Lett. **21,** 1725 (2009).
11. Y. Gong, T. Zhao, Y. Rao, Y. Wu, and Y. Guo, Opt. Express **18,** 15844 (2010).
12. Y. Zhu and A. Wang, IEEE Photon. Technol. Lett. **17,** 447 (2005).
13. D. W. Kim, F. Shen, X. Chen, and A. Wang, Opt. Lett., **30,** 3000 (2005).
14. D. Donlagic and E. Cibula, Opt. Lett. **30,** 2071 (2005).
15. E. Cibula and D. Donlagic, Opt. Express **15,** 8719 (2007).
16. M. Ohtsu, J. Lightw. Technol. **13,** 1200 (1995).
17. C. J. Tuck, R. Hagure, and C. Doyle, Meas. Sci. Technol. **17,** 2206 (2006).
18. Y. Rao, B. Xu, Z. Ran, and Y. Gong, Chin. Phys. Lett. **27,** 024208 (2010).
19. Z. L. Ran, Y. J. Rao, W. J. Liu, X. Liao, and K. S. Chiang, Opt. Express **16,** 2252 (2008).
20. T. Wei, Y. Han, Y. Li, H. Tsai, and H. Xiao, Opt. Express **16,** 5764 (2008).